Hindawi
Shock and Vibration
Volume 2021, Article ID 9623119, 17 pages
https://doi.org/10.1155/2021/9623119

Research Article

Analysis of the Influence of Transmission Housing Elasticity on the Vibration Characteristics of Gear Shafting under Coupling Effect

Hanlin Huang, Shengping Fu, and Shanming Luo

School of Marine Equipment and Mechanical Engineering, Jimei University, Fujian 361021, China

Correspondence should be addressed to Shengping Fu; 7025370@163.com and Shanming Luo; smluo@jmu.edu.cn

Received 10 August 2021; Revised 4 November 2021; Accepted 13 November 2021; Published 29 December 2021

Academic Editor: F. Viadero

Copyright © 2021 Hanlin Huang et al. This is an open access article distributed under the Creative Commons Attribution License, which permits unrestricted use, distribution, and reproduction in any medium, provided the original work is properly cited.

The influences of transmission housing elastic deformations on the vibration gear shafting characteristics are studied. The vibration model of the vehicle transmission system in consideration of the dynamics coupling of the housing and the gear shafting is constructed. Aiming at a vehicle transmission, the mathematical model of the bending and torsional gear shafting vibrations is established based on the lumped mass method. Following the elastic treatment of the box, a comprehensive stiffness model at the bearing considering the housing deformation is proposed to achieve the dynamic coupling between the box and the gear shafting system. Furthermore, the gear shafting vibration characteristics considering housing deformations are obtained by integrating multisource dynamic excitation, which is solved using an iterative method. The results are verified through a bench test. And, it shows that the elastic deformation of the housing aggravates the gear shafting vibration (bending and torsional coupled vibration). The peak frequency mostly remains the same. The maximum speed changes amplitude and associated root mean square value (calculated at the gear position) increase by 55.5% and 59.6%, respectively. Next, the maximum bearing support force and its root mean square value are increased by 63.7% and 97.6%, respectively. Finally, the largest increase in maximum vibration acceleration at the measuring point and the simulated root mean square value are 90% and 63.1%, respectively. It is concluded that the research results provide a theoretical basis for the study of transmission dynamic reliability.

1. Introduction

Gear transmission displays complex dynamics behaviors, which are the result of both internal and external multisource excitations. The dynamic gear shafting excitation deforms the thin-walled housing, and the elastic deformation is fed back to the gear shafting through bearings. As such, it affects the bending and torsional vibration characteristics of the gear shafting, reducing the vehicle NVH performance, causing resonance, and reducing the personal safety of the passengers. Thus, it is important for transmission system dynamics to establish the coupling vibration model of gearbox housing and gear shafting, which will enable analyzing the influence of elastic gearbox deformation on the dynamics characteristics of gear shifting.

At present, finite element modeling [1–4] and multibody dynamics simulations [5–9] were predominantly used in studies on transmission system dynamics. The former, finite element method, with high accuracy was used to observe various complex shapes [10–14] and simulate the quasistatic contact force in the system. However, in practical application, the transmission system is usually operated under dynamic conditions. Therefore, it is difficult to determine and set the model parameters. The nonlinearity is prominent, and the results easily diverge.

On the other hand, dynamics software simulation mitigated the test condition limitations and was fast and efficient. At the same time, the research and development cycle was shortened [15–21]. But it is mainly based on the mature commercial software. Parameter setting and incentive conditions are relatively simple, the model accuracy is limited, and deviations from the actual situation are significant.

Owing to a large number of components and complex operating conditions of the transmission, vibration characteristics research remains difficult. However, it is still the

focus of current studies. An increasing number of scholars study the interactions between housing and shafting during the transmission operation. Therefore, starting from different viewpoints, the coupling dynamics transmission system models are established to analyze the transmission system dynamic characteristics.

Liu et al. [22] observed the influences of transmission support bearing on the gear shafting vibration characteristics, establishing a gear bearing system model. Furthermore, Zhang et al. [23] determined that the excitation causing the housing deformation and the vibration was caused by the dynamic force at the bearing. Ren et al. [24] analyzed the elastic deformation and associated housing vibrations through the rigid-flexible coupling of the gear shafting and the housing. Additionally, the literature [25, 26] based on the rigid-flexible coupling theory was available, including the coupling model of the transmission system and the housing. Next, Jiang et al. [27] used the lumped mass method to separate the system into several mass points, establishing the coupling model of the housing and the gear shafting system.

Although the dynamics coupling of housing and gear shafting were considered in the above-presented studies, a specific model for the coupling part analysis was not established. Furthermore, there were few studies on the influence of elastic gearbox housing deformation on gear shafting vibrations.

In this paper, a vehicle transmission is viewed as the research object, and the comprehensive stiffness model of bearings is established considering the housing elasticity at the coupling part between the housing and the shafting. Furthermore, the dynamics coupling model of the transmission housing and gear shafting is established and solved via the Simulink and ADAMS cosimulation method. The model is verified using a bench test, and the profound influences of housing elastic deformations on the gear shafting dynamic characteristics are analyzed.

2. Research Object

A two-stage and three-axis vehicle gearbox is selected as the research object, as shown in Figure 1. The transmission diagram is shown in Figure 2. The right side of the figure shows the schematic diagram of transmission meshing gear in each gear position.

The bearing models and gear parameters in Figure 2 are shown in Table 1 and 2, respectively.

3. Bending and Torsional Coupled Vibration Model of Gear Shafting

3.1. Simulink Model. The bending and torsional coupled vibration model of gear shafting model is established via the lumped mass method, as shown in Figure 3. The following assumptions are required:

(1) Gear and bearing are taken as mass points

(2) The transmission shafting is simplified as a simply supported beam

(3) The frictions at the meshing point are all ignored

The dynamics equation of bearing mass point is as follows:

$$\begin{cases} m_{bi}\ddot{x}_h + \mathbf{K}_h(i,:)X_h + C_h(i,:)\dot{X}_h + k_{bi}x_h + c_{bi}\dot{x}_h = 0, \\ m_{bi}\ddot{y}_h + \mathbf{K}_h(i,:)Y_h + C_h(i,:)\dot{Y}_h + k_{bi}y_h + c_{bi}\dot{y}_h = 0, \\ J_{bh}\ddot{\theta}_i + k_{i-j}\left(\theta_i - \theta_j\right) + c_{i-j}\left(\dot{\theta}_i - \dot{\theta}_j\right) = 0. \end{cases} \tag{1}$$

The dynamics equation of gear mass point is as follows:

$$\begin{cases} m_i\ddot{x}_i + \mathbf{K}_1(i,:)X_1 + \mathbf{C}_h(i,:)\dot{X}_h + k_{mi}\cdot\left(R_i\theta_i - R_j\theta_j\right) - c_{mi}\cdot\left(R_i\dot{\theta}_i - R_j\dot{\theta}_j\right) = 0, \\ m_i\ddot{y}_i + \mathbf{K}_1(i,:)Y_1 + \mathbf{C}_h(i,:)\dot{Y}_h + k_{mi}\cdot\left(R_i\theta_i - R_j\theta_j\right) + c_{mi}\cdot\left(R_i\dot{\theta}_i - R_j\dot{\theta}_j\right) = 0, \\ J_i\ddot{\theta}_i + k_{i-j}\left(\theta_i - \theta_j\right) + c_{i-j}\left(\dot{\theta}_i - \dot{\theta}_j\right) + k_{i-j}\left(\theta_i - \theta_j\right) + c_{i-j}\left(\dot{\theta}_i - \dot{\theta}_j\right) \\ + k_{mi}\cdot\left(R_i\theta_i - R_j\theta_j\right)\cdot R_i + c_{mi}\cdot\left(R_i\dot{\theta}_i - R_j\dot{\theta}_j\right)\cdot R_i = 0, \end{cases} \tag{2}$$

where K_h is the bending stiffness matrix of the h-th axis, C_h is the bending damping matrix of the h-th axis, subscript b represents the bearing related symbols, subscript m represents the gear meshing pair related symbols, m_{bi} is the bearing mass at mass point i, k_{bi} is the bearing stiffness at mass point i, c_{bi} is the bearing damping at mass point i, m_i is the shaft mass at mass point i, J_i is the inertia of mass point i (related to its parameters); θ_i is the shaft mass point i rotation angle, $k_{i\text{-}j}$ is the torsional stiffness of the shaft segment between mass points i and j, $c_{i\text{-}j}$ is the torsional damping between mass points i and j, k_m is the meshing stiffness, and c_m is the meshing damping.

The model of each bearing is shown in Table 1. The bearing support stiffness calculation method [28] is used. The stiffness is related to speed and increases with the increase in speed. The support stiffness of each bearing at the engine speed of 2000 r/min is shown in Table 3.

The transmission shaft is simplified as a multisupport continuous beam, while the bearing and gear are represented as some discrete mass points, as shown in Figure 4. Furthermore, the shaft segment between the mass points is regarded as an elastic element. Finally, the transmission shaft bending stiffness matrix is solved via material mechanics.

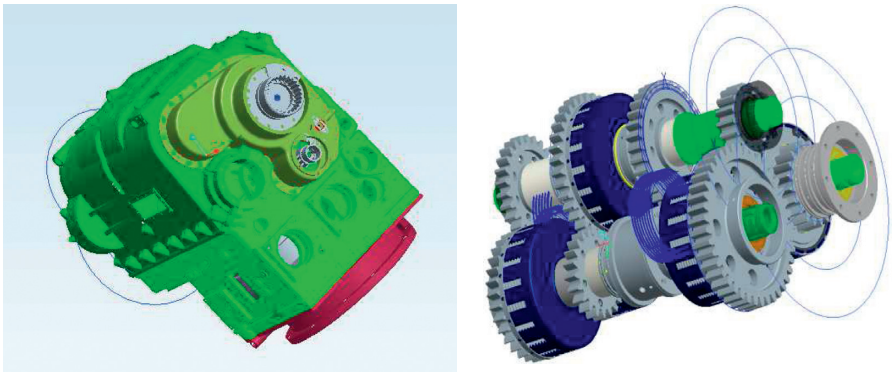

(a) (b)

Figure 1: Transmission Model. (a) Transmission housing model. (b) Gear shafting models.

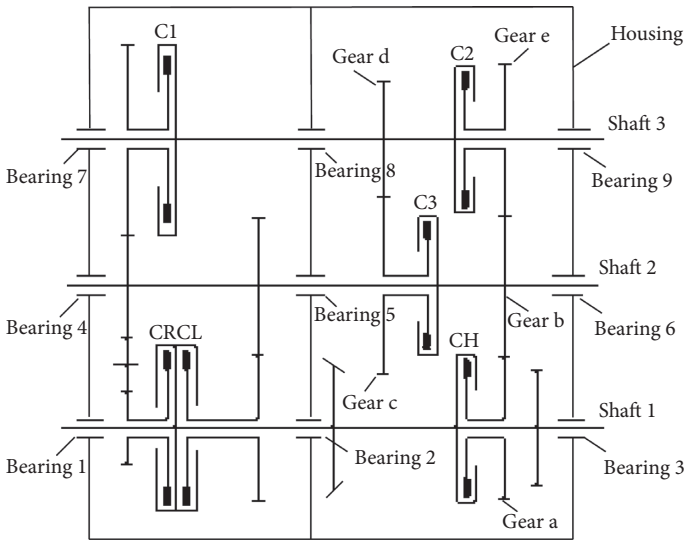

	1	2	3	4	5	6	-1
CL	+		+		+		
CH		+	+			+	
CR							+
C1	+	+					+
C2			+	+			
C3					+	+	

Figure 2: Transmission system schematic diagram.

Table 1: Bearing model.

Bearing designation	Model	Bearing number	Model
Bearing 1	QJ311	Bearing 6	QJ311
Bearing 2	QJ313	Bearing 7	SKF6217
Bearing 3	QJ311	Bearing 8	SKF6314
Bearing 4	SKF QJ311	Bearing 9	SKF6217
Bearing 5	22214E		

Table 2: Gear parameters.

Number of gear	Gear A	Gear B	Gear C	Gear D	Gear E
Gear module, m	7	7	7	7	7
Teeth number, Z	33	26	17	37	31
Modification coefficient, x	-0.3	0.3	0.35	0.3	0.23
Pressure angle, λ (°)	20	20	20	20	20
Addendum, h_1 (mm)	4.9	8.89	8.95	9.1	8.4
Full tooth height, h (mm)	15.75	15.54	15.25	15.75	15.54
Accuracy class	7GJ	7GJ	7GJ	7GJ	7GJ

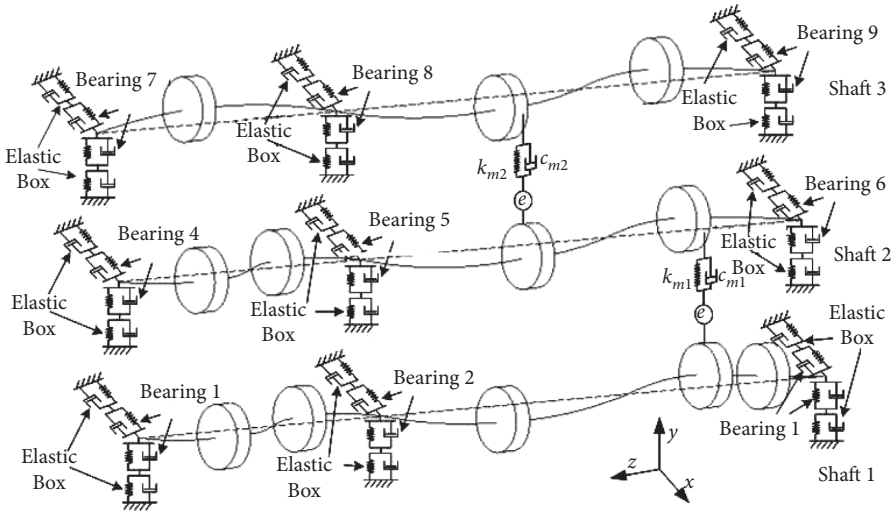

Figure 3: Mechanical model diagram of gear shafting.

Table 3: Bearing stiffnesses.

Transmission shaft	Left side bearing (N/mm)	Intermediate bearing (N/mm)	Right side bearing (N/mm)
Shaft 1	51800	83800	92500
Shaft 2	3470	41900	33400
Shaft 3	95300	61900	14300

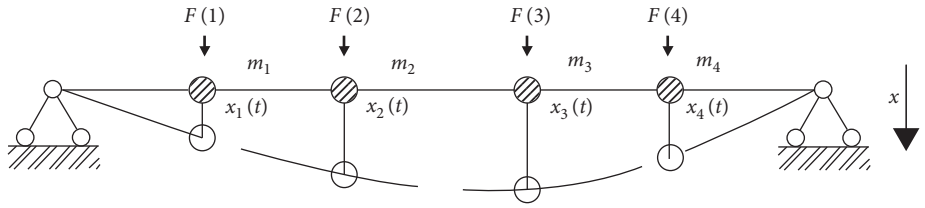

Figure 4: The equivalent multidegree of freedom bearing system.

Based on the bending and torsional coupled vibration model of the gear shafting, the Simulink model is created in MATLAB. The model includes both the torsional and bending vibration model of gear shafting, as shown in Figure 5.

3.2. Time-Varying Mesh Excitation. Gear mesh dynamic excitation is also the main internal excitation, causing the vibration of the transmission housing. The gear supposed as an ideal model, created by ignoring the impact generated during the gear alternation process. The parametric excitation caused by meshing stiffness is mainly discussed.

Spur gear teeth are generally treated as two-dimensional plane problems. The corresponding calculation methods of loaded elastic deformation include the finite element method, mathematical elasticity method, and numerical method. Since the development of the numerical method, it is widely used and popularized by other scholars, mostly due to its high calculation efficiency and good agreement with the finite element method results [29–31].

Therefore, the gear mesh stiffness calculation proposed in literature [32] is adopted. It is considered that the comprehensive elastic deformation of meshing teeth is composed of cantilever beam bending, shear deformation, and the additional deformation caused by the foundation elastic deformation and tooth surface meshing contact deformation.

$$k_m = \frac{F_i}{\delta_{pi} + \delta_{gi}}, \tag{3}$$

where F_i is the force transmitted by the gear and δ_{pi} and δ_{gi} are comprehensive elastic deformation of active and passive gear meshing considering the influence of gear speed fluctuation, respectively.

The viscous meshing force is formed by multiplying the meshing damping between teeth by the dynamic transmission error. Referring to the literature, the meshing damping expression is obtained:

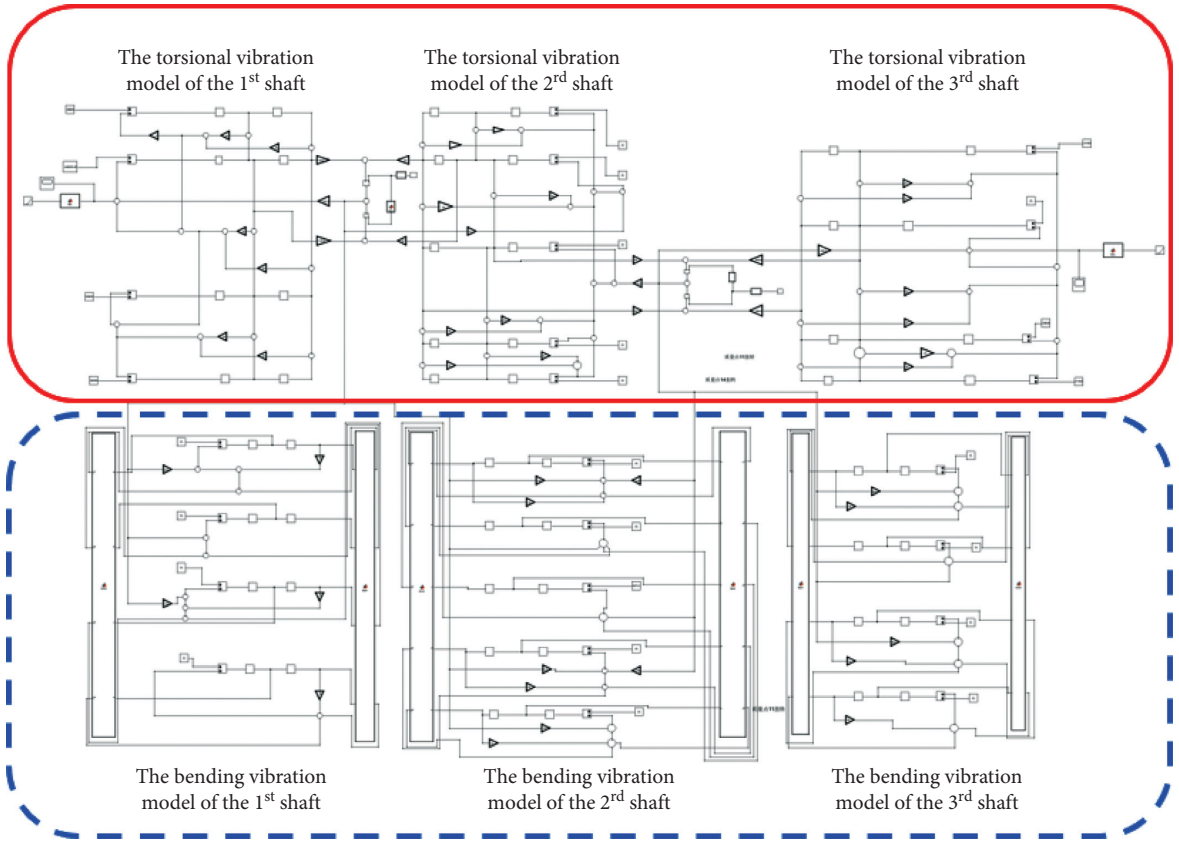

Figure 5: The Simulink model.

$$c_m = 2\xi\sqrt{\frac{k_m R R_{pg} J_p J_g}{R_p^2 J_p + R_g^2 J_g}}, \tag{4}$$

where ζ is the damping ratio of gear tooth meshing (generally 0.03–0.17; in this paper, the authors used 0.01), J_p and J_g are the moment of inertia of driving gear and driven gear, respectively, and R_p and R_g are the base circle elastic of driving and driven gear, respectively.

4. Model of the Housing

4.1. Modal Analysis. As shown in Figure 1(a), the transmission housing is an irregular thin-walled part with a complex structure. Moreover, the housing wall thicknesses are not consistent. Thus, aiming to divide the grid more accurately, the housing structure is simplified: (1) the auxiliary features needed for the assembly, such as bosses and chamfers, are ignored; (2) small parts with complex structures which have minimal influence on the analysis results are eliminated, including the bearing covers and suspension supports, among others.

The 3D model of the transmission is imported into the finite element software, and the finite element mesh is generated. Using the hexahedral dominant mesh generation method, a total of 1057019 nodes and 306469 elements are obtained, as shown in Figure 6.

The elastic characteristics of the housing are represented by modal parameters according to the substructure modal synthesis method. The modal analysis results show that the housing frequency is relatively dense. The housing natural frequency of each mode is shown in Figure 7. The first six modes are rigid.

As shown in Figure 8, the middle of the upper and lower housing segment, the right rib plate, and the transmission bearing seat hole are all relatively weak, where the deformation is more noticeable compared to other positions. Thus, those positions are adopted as measuring points for tests and simulations.

4.2. Housing Dynamics Model. The elastic housing model is imported into the dynamics software. Add a fixed constraint at the support position as shown in Figure 9. An interface node fixedly connected with the housing is established in the center of the bearing seat as the stress point of the bearing support force. The dynamics analysis model of gearbox housing is established, as shown in Figure 10.

5. Coupling Dynamics Modeling of Gearbox

Because the gear shafting is connected with the housing through bearings, meaning that the dynamic gear shafting excitation will cause deformation of the thin-walled housing. Furthermore, the elastic gearbox deformation will be fed

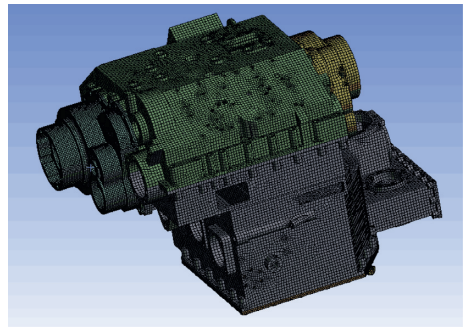

Figure 6: Housing finite element model.

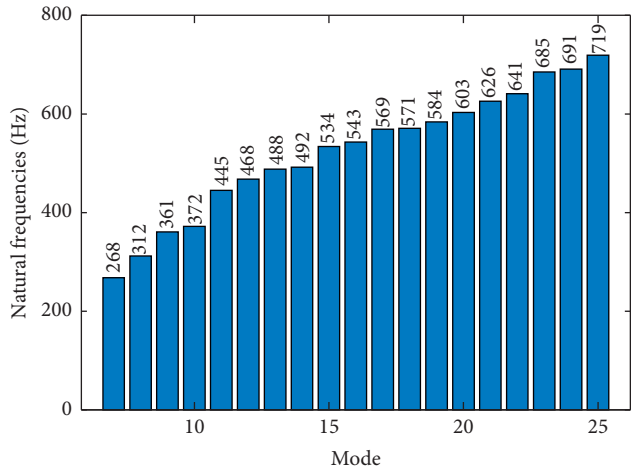

Figure 7: Housing natural frequency.

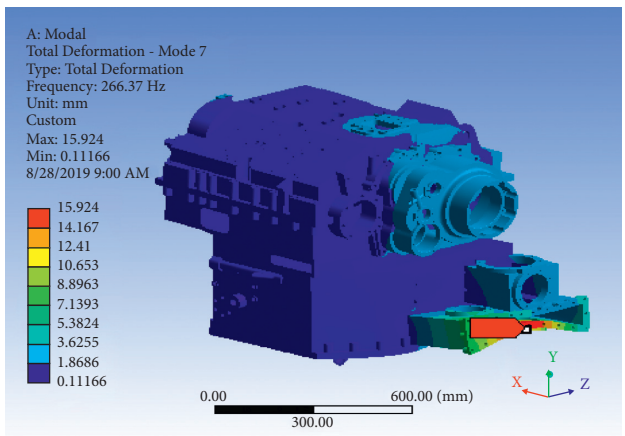

(a)

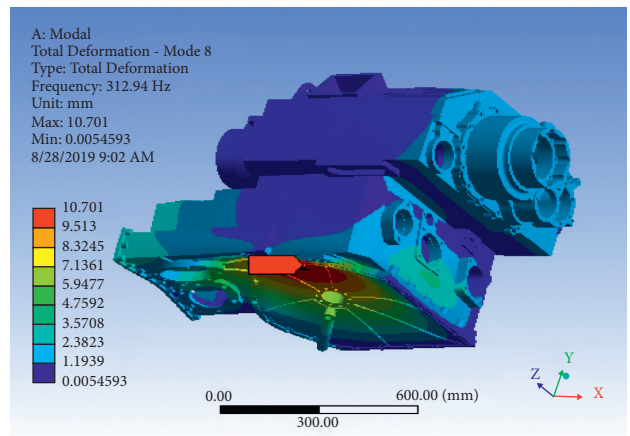

(b)

Figure 8: Continued.

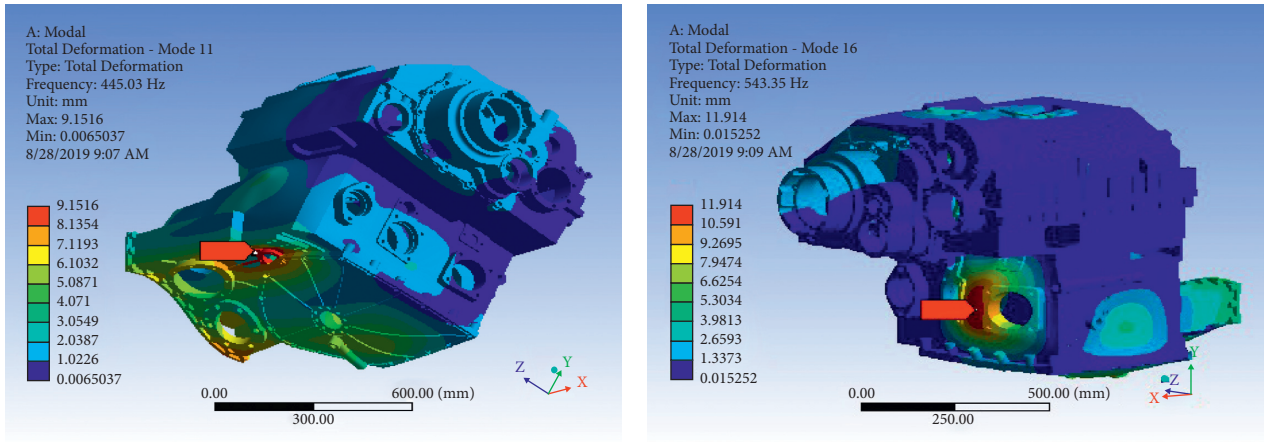

(c) (d)

Figure 8: Modal diagram of the housing. (a) The 7-th housing mode. (b) The 8-th housing mode. (c) The 11-th housing mode. (d) The 16-th housing mode.

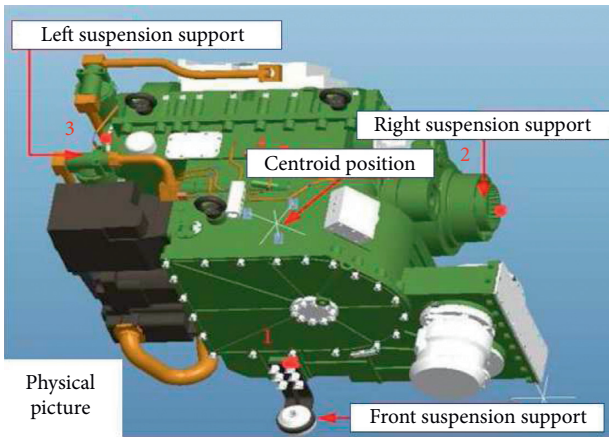

Figure 9: Fixed housing joint.

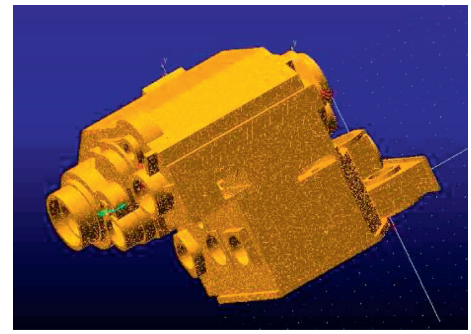

Figure 10: Housing model (ADAMS).

back to the gear shafting during the transmission operation process, affecting the gear transmission characteristics.

5.1. Dynamics Coupling Method of the Housing and Gear Shafting. The average stiffness and damping of the bearing cannot reflect its support characteristics; therefore, it is necessary to calculate both the bearing stiffness and damping in real-time, based on the bearing load and rotation state.

During the transmission working process, the dynamic gear shafting excitation deforms the thin-walled housing through bearings. Near the bearing, the housing deformation node is affected by the elastic dynamic restoring force produced by the inner bearing ring and the restoring force resulting from the outer ring stiffness. Both of the forces are driving the deformation node to the equilibrium position. The mechanical model of the comprehensive stiffness at the bearing is shown in Figure 11.

The corresponding expression for calculation of the comprehensive stiffness and damping is given as follows:

$$\begin{cases} k_b = \dfrac{k_{bj} \cdot k_x}{k_{bj} + k_x}, \\ c_b = \dfrac{c_{bj} c_x}{c_{bj} + c_x}, \end{cases} \tag{5}$$

where k_b is the comprehensive stiffness, k_{bi} is the support stiffness of the bearing (the results are given in Section 3.1), c_b is the comprehensive damping, c_{bj} is the bearing damping, c_x is the housing damping, and k_x is the housing stiffness, calculated as the ratio of the load F_Z excited by the housing at the bearing to the point shape variable s:

$$k_x = \frac{F_z}{s}. \tag{6}$$

The gear shafting bearing reaction results in the housing deformation. At the same time, the comprehensive stiffness in the consideration of the housing deformation will increase the gear shafting vibration, thus meaning that the bearing reaction and the housing deformation are influenced each other.

5.2. Solution. The comprehensive stiffness is calculated using a cosimulation. The real-time stiffness is calculated by the Simulink comprehensive stiffness solution model, which

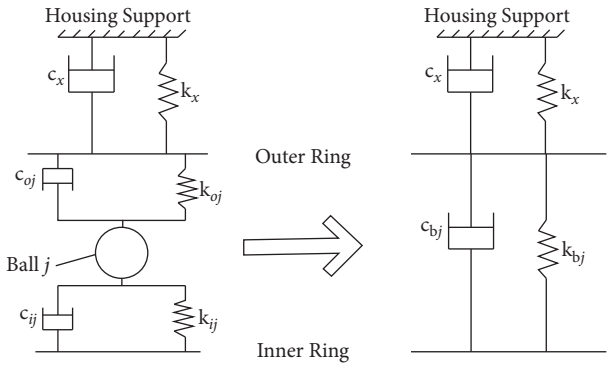

Figure 11: Comprehensive stiffness mechanical model.

is substituted into the bending torsional coupling vibration equation of gear shafting. After solving the bearing reaction force, it is substituted into ADAMS software as an input variable. The shape variable of the housing at the bearing is obtained through dynamic simulation and finally transmitted to Simulink to calculate the comprehensive stiffness. Through the information transmission between the ADAMS and Simulink, the comprehensive time-varying stiffness is obtained, as shown in Figure 12.

Interactive parameters are transmitted between the ADAMS and Simulink. Therefore, bearing reaction force is input to ADAMS/view to complete the dynamics simulation.

And, the box deformation at each of the nine bearings is input to the Simulink comprehensive stiffness calculation module as the output parameters at the same time. Initial value is set. The calculated support reaction of bearing is transmitted to the housing model. In addition, the shell deformation is transferred into the Simulink comprehensive stiffness model. The time-varying comprehensive stiffness is calculated. And, the cosimulation realizes eventually, as shown in Figure 13.

6. Experimental Verification

Aiming to evaluate both the accuracy and validity of the dynamics coupling model of the transmission housing and the gear shafting, the bench test method is used.

The housing surface acceleration response is obtained via a 4326 type three-way acceleration sensor produced by B&K company and SC10DC-UTP data acquisition equipment produced by the LMS company. The resulting data are analyzed using LMS test lab software. Based on the housing modal analysis results, weak structure points on the housing surface, having a large vibration response, are selected as measuring points, as shown in Figure 14.

Working conditions used in the experiment are as follows: the 4th gear, engine speed of 1880 r/min, load of 888 Nm, and a sampling frequency of 10000 Hz.

As shown in Figures 15–18 and Table 4, the experimental and simulation data are relatively similar in the time domain. Furthermore, the main frequency and amplitude of the two are also consistent in the frequency domain, indicating that the simulation results are consistent with the transmission vibration response under realistic working conditions. The maximum root mean square error between the test and simulation is 57% that the experimental value is larger than the simulation value.

The main cause of such a behavior is that only the internal and external excitation generated by the meshing force and engine output torque is considered in simulation. Moreover, the engine input torque data are fitted and then substituted into the simulation model in the form of function. Additionally, remaining factors that may aggravate the box vibration response, such as the excitation of the other front and rear transmission meshing gears (such as the helical gear meshing in the input shaft) and the experimental equipment lap gap is not considered.

Thus, the acceleration amplitude of the most measuring points in the time domain is relatively smaller compared to the experimental value. On the other hand, in the frequency domain, some of which are higher than the corresponding experimental values since the simulation model only considered the engine excitation and gear meshing excitation, causing the system energy concentration.

7. Analysis of the Housing Elasticity Influence on the Gear Shafting System

Under the 4th gear condition, the engine speed is 2000 r/min, and the load is 888 Nm; the resulting engine output torque is shown in Figure 19. Furthermore, the meshing stiffness of two meshing gear pairs is shown in Figure 20, where the simulation step is 0.001 s.

The vibration characteristics of gear shafting with and without the housing elastic deformation are simulated and compared.

7.1. Bending Vibration. One mass point is selected on each of the three shafts (gear A, B, and E), to observe the bending vibration characteristics of the gear shafting under two simulation conditions. As shown in Figure 21, the bending acceleration vibrates periodically with time. When the coupling between the housing and gear shafting is considered, the vibration increases significantly. The peak frequencies are practically the same and corresponded to the engine excitation frequency (200 Hz) and gear meshing frequency (1100 Hz and 1130 Hz). However, the amplitude in the coupled mode is significantly higher compared to that of the uncoupled mode.

The comparison of the bending vibration acceleration response under two simulation conditions is shown in Table 5. It shows that the bending vibration of gear shafting is more severe when considering the elastic deformation of the housing.

7.2. Torsional Vibration. The vibration speed of each mass point after removing the initial speed is shown in Figure 22. It indicates that the gear speed changes periodically with time and vibrates continuously near by the initial speed. Considering the coupling between the housing and shafting system, the speed vibration of gears has varying degrees of increase. The peak frequencies of two simulation conditions

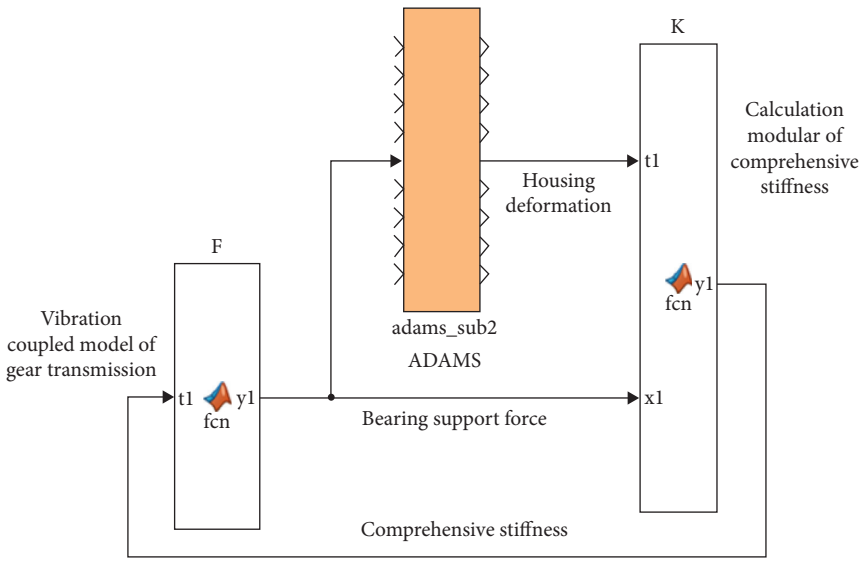

Figure 12: Comprehensive stiffness solution model (Simulink).

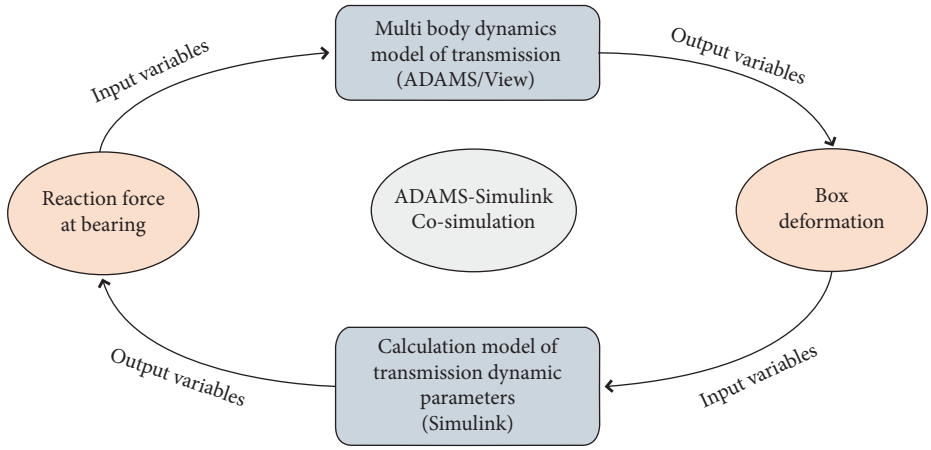

Figure 13: Schematic diagram of cosimulation.

(a) (b)

Figure 14: Continued.

(c) (d)

Figure 14: Measuring point locations. (a) Point 2 (upper part of Mount). (b) Point 3 (lower part of Mount). (c) Point 5 (top oil pipe). (d) Point 8 (easily damaged lubricating oil position).

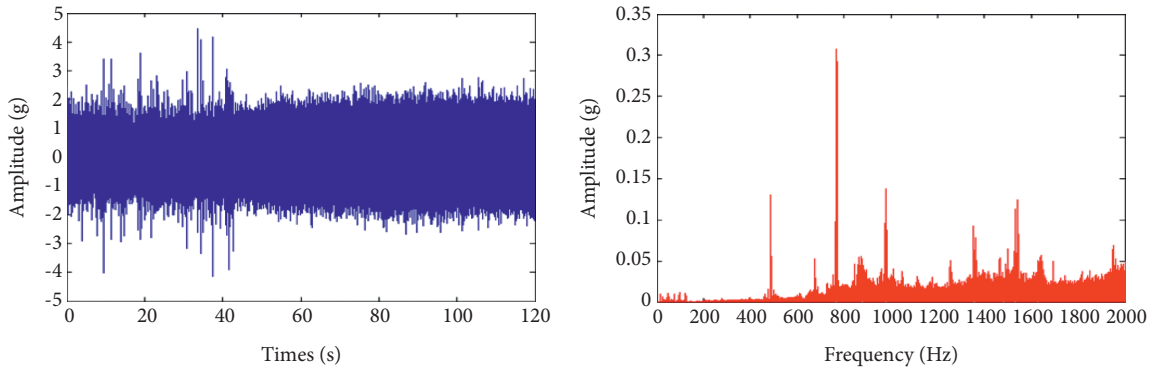

(a) (b)

Figure 15: Experimental acceleration values at measuring point 2. (a) Experimental results for time domain acceleration at measuring point 2. (b) Experimental results for frequency domain acceleration at measuring point 2.

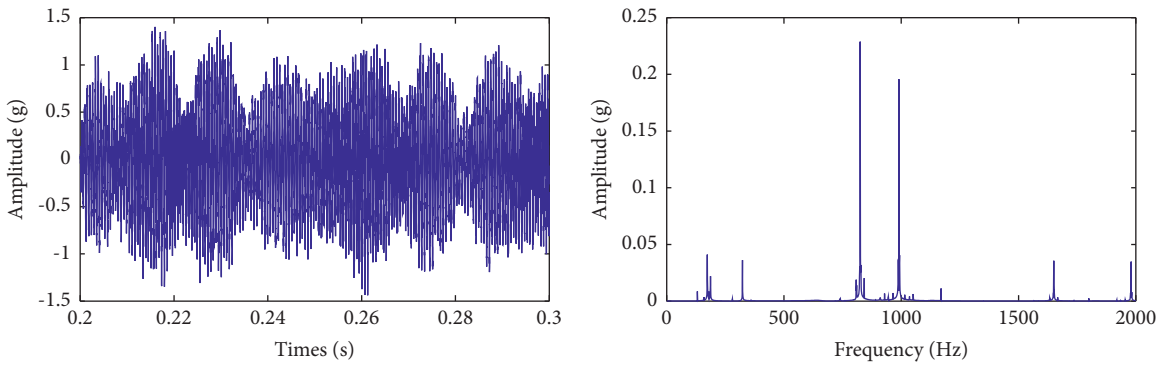

(a) (b)

Figure 16: Simulation acceleration values at measuring point 2. (a) Simulation results for time domain acceleration at measuring point 2. (b) Simulation results for frequency domain acceleration at measuring point 2.

are nearly the same and are corresponding to the engine excitation frequency (200 Hz) and gear meshing frequency (1100 Hz and 1130 Hz). The comparison of the torsional vibration response under two simulation conditions is shown in Table 6. On the other hand, the amplitude in the coupled mode is significantly higher than that of the uncoupled mode.

7.3. Bearing Support Force. The bearing support force under the two simulation conditions are shown in Figure 23. The time-domain diagram shows that the bearing support force trend is similar to that of both the torsion and vibration (it is a periodic vibration trend). In two simulation conditions, the peak frequency is rather similar and corresponded to the engine excitation frequency (200 Hz) and gear meshing

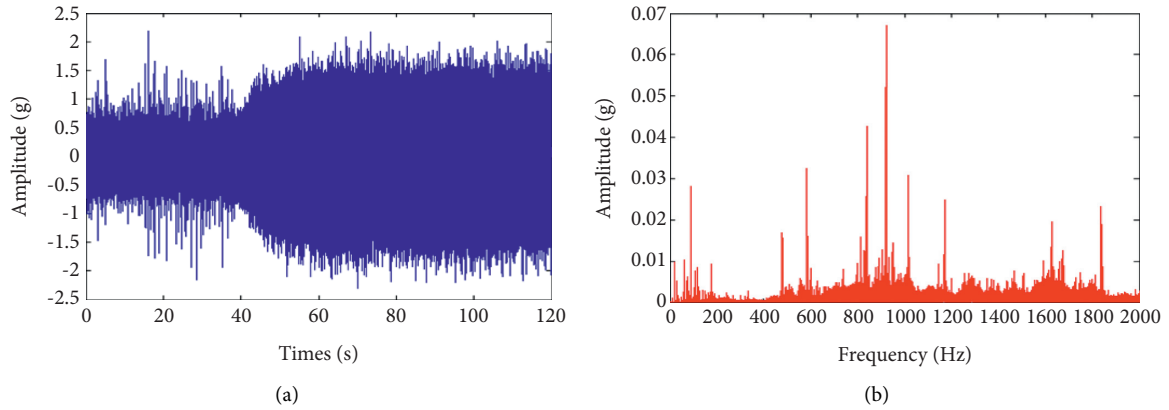

Figure 17: Experimental acceleration values at measuring point 3. (a) Experimental results for time domain acceleration at measuring point 3. (b) Experimental results for frequency domain acceleration at measuring point 3.

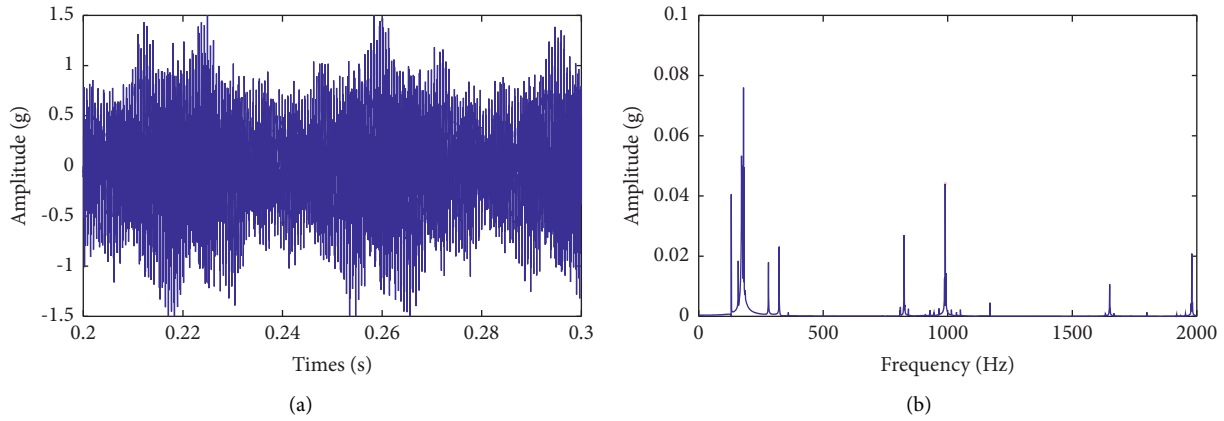

Figure 18: Simulation acceleration values at measuring point 3. (a) Simulation results for time domain acceleration at measuring point 3. (b) Simulation results for frequency domain acceleration at measuring point 3.

Table 4: Comparison of acceleration mean square values (g).

Measuring point position	2	4	5	6	8	
	0.337835	0.4103	0.937248	6.014539	9.657367	Experimental data
1500 (r/min)	0.2620	0.2982	1.2991	6.6479	4.1115	Simulation data
	22.4%	27.3%	27.8%	10.5%	57.4%	Error
	0.415739	0.389005	1.081859	6.088278	10.44699	Experimental data
1800 (r/min)	0.2473	0.2648	1.0028	4.2336	5.0406	Simulation data
	40.5%	31.5%	7.3%	30.4%	51.7%	Error

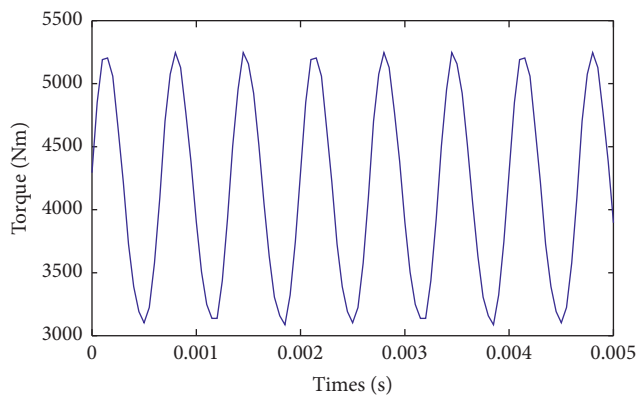

Figure 19: Engine output torque.

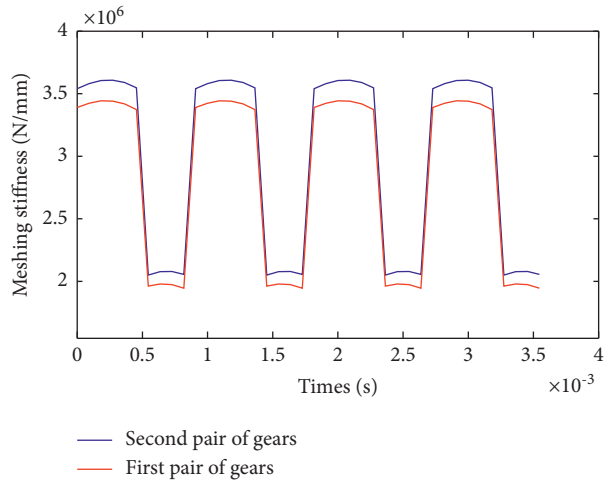

Figure 20: Meshing stiffness of two meshing gear pairs.

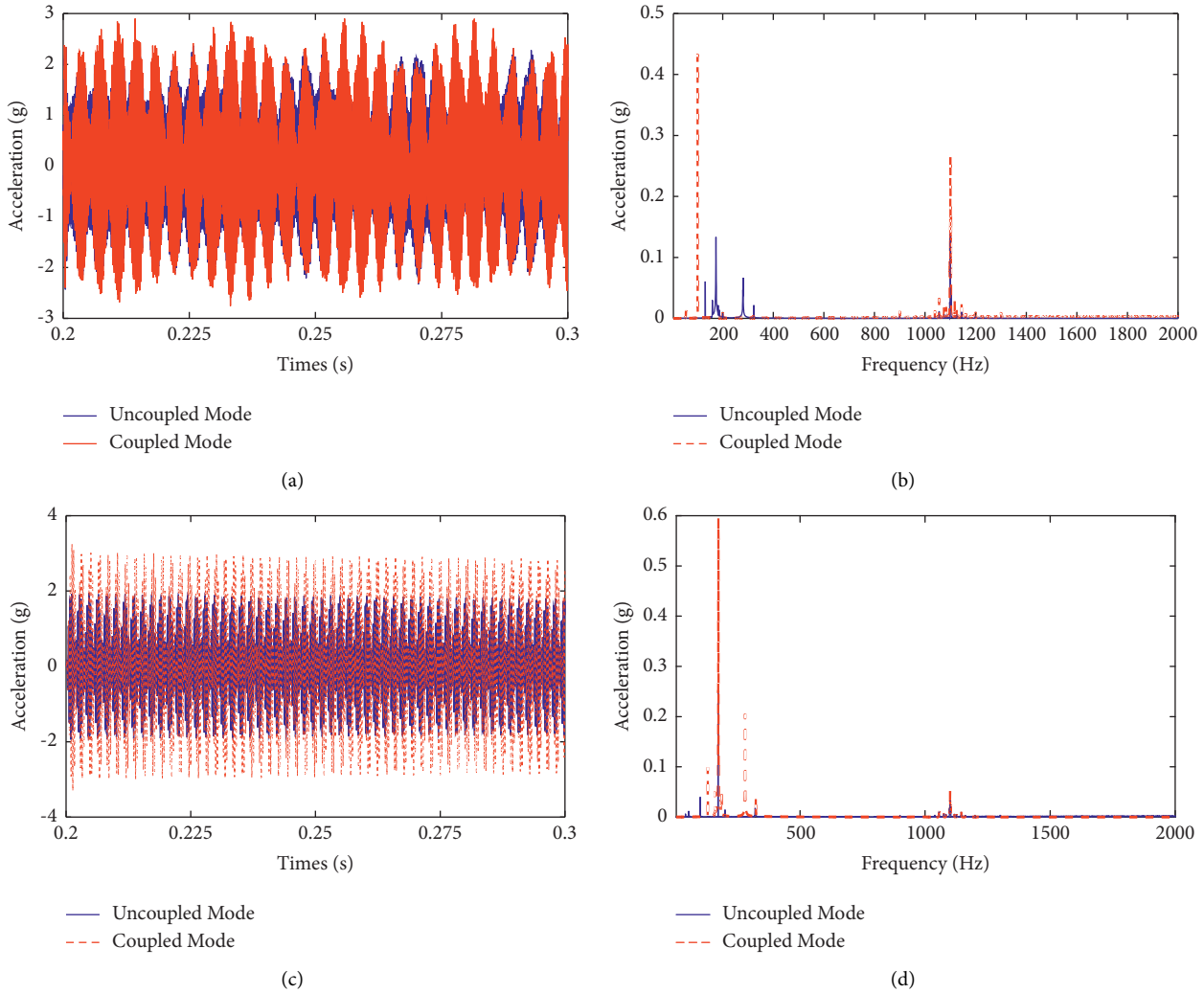

Figure 21: Continued.

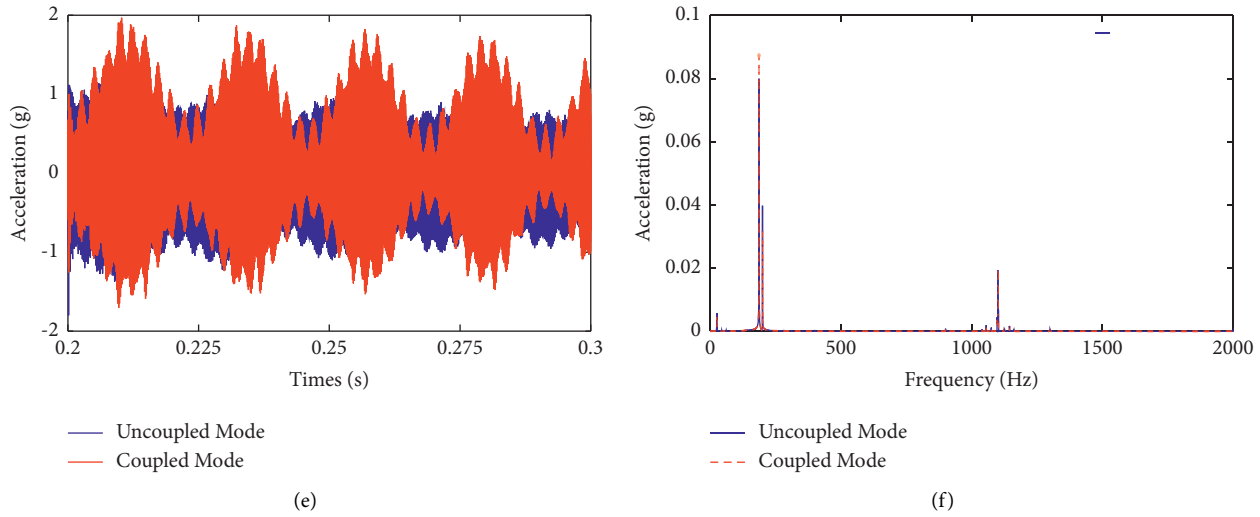

Figure 21: Influences of housing elasticity on the mass point bending vibration characteristics. (a) Bending vibration acceleration of gear A in the time domain. (b) Bending vibration acceleration of gear A in the frequency domain. (c) Bending vibration acceleration of gear B in the time domain. (d) Bending vibration acceleration of gear B in the frequency domain. (e) Bending vibration acceleration of gear E in the time domain. (f) Bending vibration acceleration of gear E in the frequency domain.

Table 5: Comparison of mass point bending vibration acceleration responses.

	Gear A	Gear B	Gear E	
Maximum vibration acceleration(g)	3.87	4.02	2.44	Coupling model
	2.18	2.11	1.63	Uncoupling model
	77.2%	90.1%	49.7%	Increase
Root mean square value of vibration acceleration (g)	1.32	1.99	0.91	Coupling model
	0.88	1.22	0.64	Uncoupling model
	50%	63.1%	42.2%	Increase

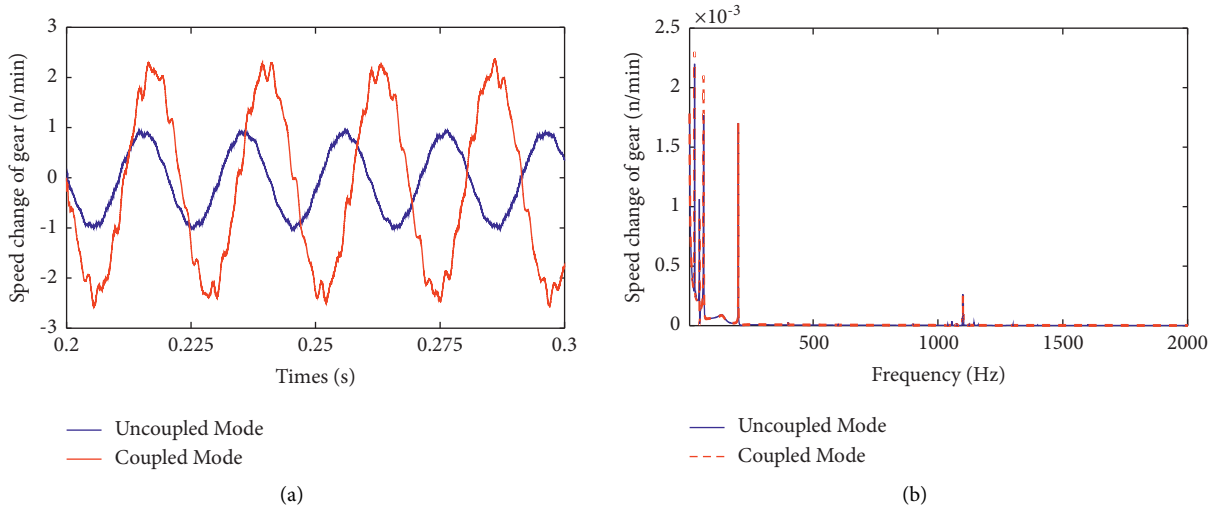

Figure 22: Continued.

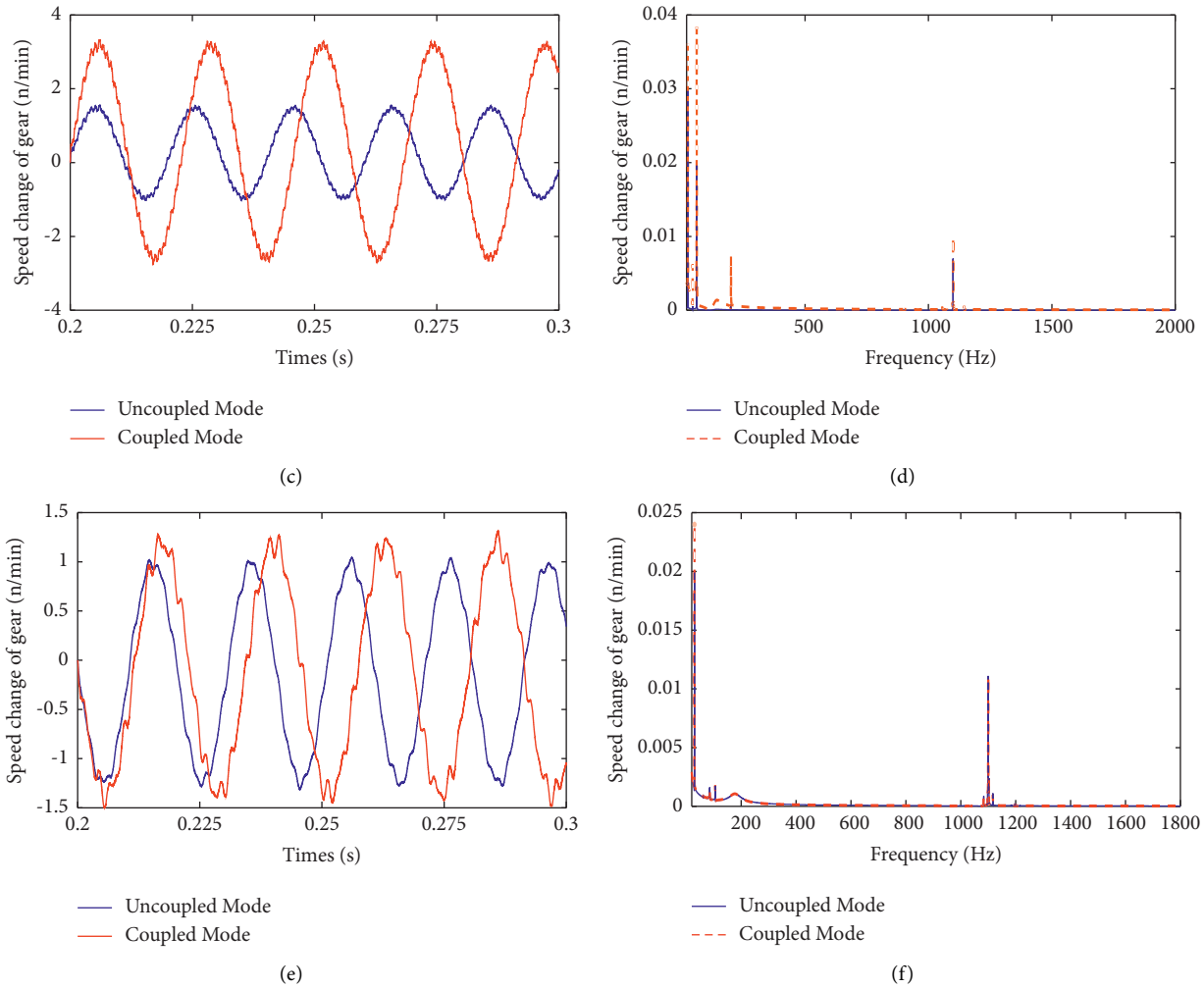

Figure 22: The mass point torsional vibration response in two simulation conditions. (a) Time-domain diagram of gear A speed. (b) Frequency domain diagram of gear A speed. (c) Time-domain diagram of gear B speed. (d) Frequency domain diagram of gear B speed. (e) Time-domain diagram of gear E speed. (f) Frequency domain diagram of gear E speed.

Table 6: Comparison of torsional vibration responses.

	Gear A	Gear B	Gear E	
Maximum speed change (r/min)	2.81	3.88	1.61	Coupling model
	1.25	1.84	1.37	Uncoupling model
	55.5%	52.6%	14.9%	Increase
Root mean square value of speed change(r/min)	1.93	2.49	1.09	Coupling model
	0.78	1.22	0.84	Uncoupling model
	59.6%	51%	22.9%	Increase

frequency (1100 Hz and 1130 Hz). After the gear shafting is coupled with the housing, the bear support force increases and the vibration intensifies. It indicates that the elastic deformation of the housing intensifies the gear meshing impact, increasing the fluctuation of bearing support force amplitude at the bearing. The phenomenon reflects of the bearing support force is more consistent with the actual vibration situation.

As shown in Table 7, the maximum increase of the measured point support force and the maximum increase of the root mean square value in the simulation are 63.7% and 97.6%, respectively. Additionally, data in the coupling mode are larger than those obtained for the uncoupled mode.

In summary, due to the introduction of the elastic deformation characteristics of the housing, the comprehensive bearing stiffness replaced its original counterpart and the housing. Therefore, the gear shafting displays a larger radial displacement based on the bending deformation. In other words, the elastic characteristics of the housing intensify the impact of the gear shafting bending vibrations, while their impact on the torsional vibration is limited.

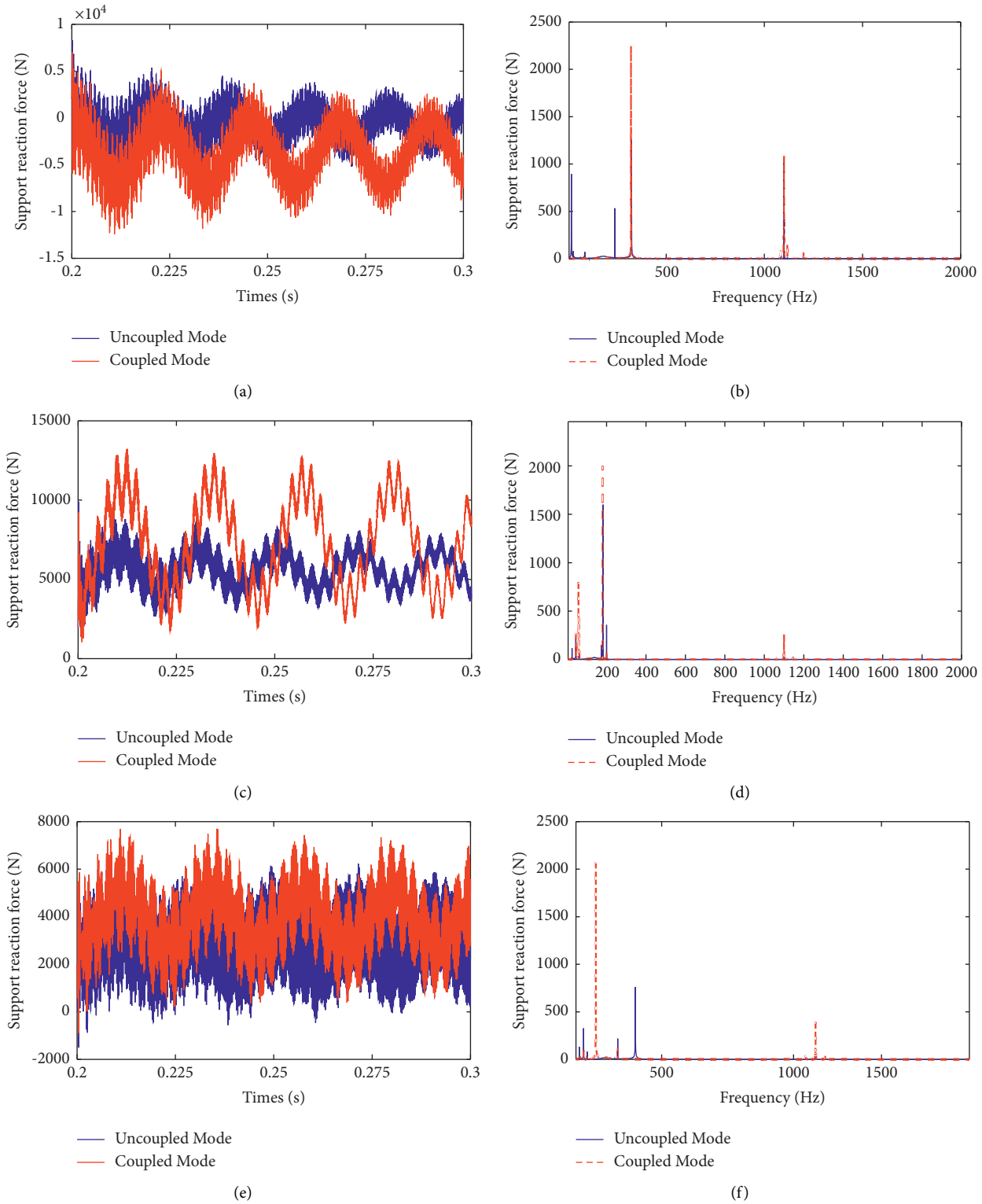

Figure 23: The bearing support force in two modes. (a) Time-domain diagram of bearing 1 support force. (b) Frequency domain diagram of bearing 1 support force. (c) Time-domain diagram of bearing 5 support force. (d) Frequency domain diagram of bearing 5 support force. (e) Time-domain diagram of bearing 9 support force. (f) Frequency domain diagram of bearing 9 support force.

Table 7: Comparison of bearing support force.

	Bearing 1	Bearing 5	Bearing 9	
Maximum support reaction (g)	15606	13784	6834	Coupling model
	8709	8783	4221	Uncoupling model
	55.4%	63.7%	61.7%	Increase
Root mean square value of support reaction (g)	9107	6642	2883	Coupling model
	4607	4214	1939	Uncoupling model
	97.6%	63.4%	67.2%	Increase

8. Conclusion

(1) The housing deformation caused by the bearing reaction force is calculated based on its elasticity. Considering the housing elasticity, the calculation model of the comprehensive time-varying stiffness at the bearing point is established. Additionally, the coupling method between the transmission housing and the gear shafting system is proposed.

(2) The calculation model for calculating the gear shifting vibration characteristics considering the housing elasticity is established. The bench test is designed and carried out to verify the simulation model. The results have shown that the variation trends obtained by the two methods are consistent in the time domain. The influence of vertical excitation, test noise, and simulation assumption conditions are not considered in the simulation modeling, resulting in lower values for simulation results. The associated maximum root mean square error is 57%.

(3) The coupling vibration model of the transmission gear shafting system and housing is simulated, and the dynamic characteristics of gear shafting considering elastic deformation are compared and analyzed. The results have shown that the housing deformation significantly affects the dynamic gear shafting system characteristics. Further, the bending and torsional vibration trend of the transmission shafting and bearing support force has varying degrees of increase. The maximum increases of bearing support force at the measuring point and the simulated root mean square value are 63.7% and 97.6%, respectively. The largest increase in maximum vibration acceleration at the measuring point and the simulated root mean square value are 90% and 63.1%, respectively. Based on the results, it is concluded that research results provide the theoretical support required for the reliability analysis of vehicle transmission.

Data Availability

The data used to support the findings of this study are available from the corresponding author upon request.

Conflicts of Interest

The authors declare that they have no conflicts of interest regarding the publication of this paper.

Acknowledgments

This work was partially supported by the National Natural Science Function of China (grant nos. 51975500 and 51975499) and the Natural Science Function of Fujian Province, China (grant no. 2019J01862). The authors would like to express their gratitude to the financial support.

References

[1] J. Helsen, F. Vanhollebeke, B. Marrant, D. Vandepitte, and W. Desmet, "Multibody modelling of varying complexity for modal behaviour analysis of wind turbine gearboxes," *Renewable Energy*, vol. 36, no. 11, pp. 3098–3113, 2011.

[2] L. Xu, C. Zhu, H. Liu, G. Chen, and W. Long, "Dynamic characteristics and experimental study on a wind turbine gearbox," *Journal of Mechanical Science and Technology*, vol. 33, no. 1, pp. 393–402, 2019.

[3] J. Y. Han, Y. Liu, S. H. Yu, S. Zhao, and H. Ma, "Acoustic-vibration analysis of the gear-bearing-housing coupled system," *Applied Acoustics*, vol. 178, 2021.

[4] C. P. Zhang, J. Wei, S. S. Hou, and J. Zhang, "Scaling law of gear transmission system obtained from dynamic equation and finite element method," *Mechanism and Machine Theory*, vol. 159, 2021.

[5] C. Y. Su, S. H. Wang, Y. F. Liu, P. Dong, and X. Xu, "Coupled vibrations of a drive system during automatic transmission," *Advances in Mechanical Engineering*, vol. 11, no. 3, 2019.

[6] W. J. Wang, G. Q. Li, and J. C. Han, "Influence rule of dynamic stress of high-speed train gearbox housing," *Journal of Traffic and Transportation Engineering*, vol. 1, pp. 85–95, 2019.

[7] J. Liu and L. Yuan, "Vibration analysis of a flexible gearbox system considering a local fault in the outer ring of the supported ball bearing," *Journal of Vibration and Control*, vol. 27, no. 9, pp. 1063–1076, 2020.

[8] H. M. Dong, Y. M. Li, Y. Xia, and J. Wei, "Simulation analysis of 8MW wind turbine gearbox vibration characteristics," *Machinery Design & Manufacture*, vol. 4, pp. 193–197, 2015.

[9] Z. Wang, Y. Cheng, P. Allen, Z. Yin, D. Zou, and W. Zhang, "Analysis of vibration and temperature on the axle box bearing of a high-speed train," *Vehicle System Dynamics*, vol. 58, no. 10, pp. 1605–1628, 2019.

[10] H. Xu, D. Qin, C. Liu, Y. Yi, and H. Jia, "Dynamic modeling of multistage gearbox and analysis method of resonance danger path," *IEEE Access*, vol. 7, no. 99, pp. 154796–154807, 2019.

[11] Z. G. Wan, Y. Y. Zi, and Y. H. Dou, "Study on the vibration characteristics of gear system with rotor crack faults under multi-axis coupling," *Noise and Vibration Control*, vol. 39, no. 3, pp. 180–186, 2019.

[12] X. Chen, Q. Hu, and Z. Zhu, "Numerical modeling and dynamic characteristics study of coupling vibration of multistage face gearsplanetary transmission," *Mechanical Sciences*, vol. 10, no. 2, pp. 475–495, 2019.

[13] M. Yang, X. Zhou, W. Zhang, J. Ye, and Y. Hu, "A modified transfer matrix method for bending vibration of CFRP/Steel composite transmission shafting," *Archive of Applied Mechanics*, vol. 90, no. 3, pp. 603–614, 2020.

[14] Q. Hui, X. L. Xie, and Z. Y. Zhang, "Influence of electromagnetic bearings on lateral vibrations and sound radiation of a shafting-hull system," *Part M. Journal of Engineering for the Maritime Environment*, vol. 234, no. 1, pp. 245–252, 2020.

[15] K. Xu, Y. Q. Zhang, and T. F. Ming, "Research on vibration characteristics of propulsion shafting under unbalanced-misaligned coupling fault," *Journal of Physics: Conference Series*, vol. 1802, no. 2, pp. 022–048, 2021.

[16] Z. Wang, P. Allen, G. Mei, Z. Yin, Y. Cheng, and W. Zhang, "Dynamic characteristics of a high-speed train gearbox in the vehicle-track coupled system excited by wheel defects," *Proceedings of the Institution of Mechanical Engineers - Part F: Journal of Rail and Rapid Transit*, vol. 234, no. 10, pp. 1210–1226, 2019.

[17] J. Liu, R.-k. Pang, H.-W Li, and J. Xu, "Influence of support stiffness on vibrations of a planet gear system considering ring with flexible support," *Journal of Central South University*, vol. 27, no. 8, pp. 2280–2290, 2020.

[18] T. J. Lin, Z. Y. He, S. Zhong, W. Liu, and L. Sheng, "Multi-body dynamic simulation and vibro-acoustic coupling analysis of marine gearbox," *Journal of Hunan University*, vol. 42, no. 2, pp. 22–28, 2015.

[19] X. P. Li, J. X. Mo, and W. J. Pan, "Influence of fractal backlash on dynamic behavior of gear-bearing system," *Journal of Mechanical Engineering*, vol. 54, no. 9, pp. 153–160, 2018.

[20] L. H. Jin, H. Q. Dong, and F. S. Zhang, "Research on low noise method of passenger car gearbox," *Journal of Mechanical Transmission*, vol. 44, no. 10, pp. 129–135, 2020.

[21] G. C. Gao, J. C. Zhang, and W. W. Guo, "Research on vibration characteristics of EMU gearbox body based on rigid-flexible coupling mode," *Joural Of Shijiazhuang Tiedao University (Natural Science Edition)*, vol. 33, no. 2, pp. 73–80, 2020.

[22] H. Liu, C. Xiang, and S. Fu, "Research on dynamic coupled characteristics of a tracked vehicle gearbox," *International Journal of Computational Intelligence Systems*, vol. 4, no. 6, pp. 1204–1215, 2011.

[23] K. L. Zhang, Z. M. Xiao, Y. D. Zhang, and Z. T. Guo, "Dynamic simulation and experimental study of gearbox based on rigid-flexible coupling modeling," *Journal of Vibration and Shock*, vol. 39, no. 7, pp. 108–115, 2020.

[24] Y. F. Ren, S. Chang, G. Liu, L. Wu, C. Zhao, and L. Chang, "Vibration analysis of gear-housing-foundation coupled system," *Journal of South China University of Technology*, vol. 45, no. 5, pp. 38–44, 2017.

[25] Z. Chen, J. Ning, K. Wang, and W. Zhai, "An improved dynamic model of spur gear transmission considering coupling effect between gear neighboring teeth," *Nonlinear Dynamics*, vol. 106, no. 1, pp. 339–357, 2021.

[26] Z. Chen, Z. Zhou, W. Zhai, and K. Wang, "Improved analytical calculation model of spur gear mesh excitations with tooth profile deviations," *Mechanism and Machine Theory*, vol. 149, Article ID 103838, 2020.

[27] J. Jiang, Z. Chen, W. Zhai, T. Zhang, and Y. Li, "Vibration characteristics of railway locomotive induced by gear tooth root crack fault under transient conditions," *Engineering Failure Analysis*, vol. 108, Article ID 104285, 2020.

[28] C. L. Xiang, T. T. Sun, and H. Liu, "Caterpillar transmission gear inner dynamic excitation and its numerical solution," *Machinery Design & Manufacture*, vol. 1, pp. 6–8, 2010.

[29] F. Ke, A. S. Wade, B. R. Robert, H. Wu, and Z. Peng, "Vibration-based monitoring and prediction of surface profile change and pitting density in a spur gear wear process," *Mechanical Systems and Signal Processing*, vol. 165, Article ID 108319, 2022.

[30] I. Howard, S. Jia, and J. Wang, "The dynamic modelling of a spur gear in mesh including friction and a crack," *Mechanical Systems and Signal Processing*, vol. 15, no. 5, pp. 831–853, 2001.

[31] C. Yuksel and A. Kahraman, "Dynamic tooth loads of planetary gear sets having tooth profile wear," *Mechanism and Machine Theory*, vol. 39, no. 7, pp. 695–715, 2004.

[32] S. P. Fu and C. L. Xiang, "Numerical calculation of ball bearing excitation and application in multi-body dynamics simulation," in *Proceedings of the IEEE 10th International Conference on Computer-Aided Industrial Design and Conceptual Design*, pp. 596–600, Wenzhou, China, November 2009.